



Changes in multimodality functional imaging parameters early during chemoradiation predict treatment response in patients with locally advanced head and neck cancer

Kee H. Wong^{1,2} · Rafal Panek² · Alex Dunlop^{1,2} · Dualta Mcquaid¹ · Angela Riddell³ · Liam C. Welsh^{1,2} · Iain Murray⁴ · Dow-Mu Koh^{2,3} · Martin O. Leach^{2,5} · Shreerang A. Bhide^{1,2} · Christopher M. Nutting^{1,2} · Wim J. Oyen^{2,4} · Kevin J. Harrington^{1,2} · Kate L. Newbold^{1,2}

Received: 20 September 2017 / Accepted: 13 November 2017

© The Author(s) 2017. This article is an open access publication

Abstract

Objective To assess the optimal timing and predictive value of early intra-treatment changes in multimodality functional and molecular imaging (FMI) parameters as biomarkers for clinical remission in patients receiving chemoradiation for head and neck squamous cell carcinoma (HNSCC).

Methods Thirty-five patients with stage III-IVb (AJCC 7th edition) HNSCC prospectively underwent ¹⁸F-FDG-PET/CT, and diffusion-weighted (DW), dynamic contrast-enhanced (DCE) and susceptibility-weighted MRI at baseline, week 1 and week 2 of chemoradiation. Patients with evidence of persistent or recurrent disease during follow-up were classed as non-responders. Changes in FMI parameters at week 1 and week 2 were compared between responders and non-responders with the Mann-Whitney U test. The significance threshold was set at a *p* value of <0.05.

Results There were 27 responders and 8 non-responders. Responders showed a greater reduction in PET-derived tumor total lesion glycolysis (TLG_{40%}; *p* = 0.007) and maximum standardized uptake value (SUV_{max}; *p* = 0.034) after week 1 than non-responders but these differences were absent by week 2. In contrast, it was not until week 2 that MRI-derived parameters were able to discriminate between the two groups: larger fractional increases in primary tumor apparent diffusion coefficient (ADC; *p* < 0.001), volume transfer constant (K^{trans}; *p* = 0.012) and interstitial space volume fraction (V_e; *p* = 0.047) were observed in responders versus non-responders. ADC was the most powerful predictor ($\Delta >17\%$, AUC 0.937).

Conclusion Early intra-treatment changes in FDG-PET, DW and DCE MRI-derived parameters are predictive of ultimate response to chemoradiation in HNSCC. However, the optimal timing for assessment with FDG-PET parameters (week 1) differed from MRI parameters (week 2). This highlighted the importance of scanning time points for the design of FMI risk-stratified interventional studies.

Electronic supplementary material The online version of this article (<https://doi.org/10.1007/s00259-017-3890-2>) contains supplementary material, which is available to authorized users.

Keywords Head and neck squamous cell carcinoma · MRI · PET/CT · Chemoradiation · Biomarker

✉ Kee H. Wong
kee.wong@icr.ac.uk

¹ Head and Neck Unit, The Royal Marsden NHS Foundation Trust, Downs Road, Sutton SM2 5PT, UK

² Radiotherapy and Imaging Division, The Institute of Cancer Research, London, UK

³ Clinical Radiology, The Royal Marsden NHS Foundation Trust, Sutton, UK

⁴ Nuclear Medicine, The Royal Marsden NHS Foundation Trust, Sutton, UK

⁵ CRUK Cancer Imaging Centre, The Institute of Cancer Research and the Royal Marsden NHS Foundation Trust, London, UK

Introduction

Radical chemoradiation (CRT) is widely accepted as the standard of care for organ-sparing treatment of locally advanced head and neck squamous cell carcinoma (HNSCC). However, it is now evident that locally advanced HNSCC represents a disease spectrum rather than a single entity, with variable response to standard CRT. Clinical variables such as tumor, node and metastases (TNM) staging and smoking history are prognostically robust but predictively deficient. Reliable prediction of outcome early during CRT is, therefore, highly desirable to avoid continuation of ineffective treatment and guide adaptation of therapy based on response.

Functional and molecular imaging (FMI) can characterize tumor phenotypes by providing quantitative parameters with radiobiological relevance. ^{18}F -FDG-PET/CT and MRI both have the benefit of being non-invasive, allowing serial measurements during radiotherapy. Several correlation studies in HNSCC have demonstrated varied, but complementary, biological information from different FMI parameters [1, 2]. To date, most FMI biomarker studies in HNSCC have concentrated only on pre-treatment time points. Indeed, there remains a paucity of prospective data to define the optimal time point for early intra-treatment assessment in patients receiving CRT.

Here, we report the results of serial ^{18}F -FDG-PET/CT, and diffusion-weighted (DW), dynamic contrast-enhanced (DCE) and susceptibility-weighted (SW) MRI following the first and second week of CRT in patients with HNSCC. The primary objective of this analysis is to identify the optimal timing and predictive value of early intra-treatment changes in FMI parameters for ultimate response to CRT.

Materials and methods

Study design

Patients with previously untreated histologically proven HNSCC (AJCC 7th edition stage III-IVb) and WHO performance status 0–2 planned for CRT, were eligible for the study. Forty patients were recruited at our institution between April 2014 and August 2016. This study received approvals from the institutional review board (CCR3926) and research ethical committee (13/LO/0067). All patients provided written consent.

Patients were treated with 6 weeks of radiotherapy with concomitant chemotherapy [cisplatin (100 mg/m²) or carboplatin (AUC5) days 1 and 29]. Macroscopic and microscopic disease received 65 Gy and 54 Gy in 30 fractions, respectively, using intensity-modulated radiotherapy with a simultaneous integrated boost technique.

Patients prospectively underwent ^{18}F -FDG-PET/CT, DW, SW and DCE MRI at baseline, week 1 (after the 4th or 5th fraction) and week 2 (after the 9th or 10th fraction) during treatment. Response was assessed at 3 months following completion of CRT with MRI, ^{18}F -FDG-PET/CT and clinical examination including nasendoscopy. Patients with evidence of residual disease at 3 months were discussed in the multidisciplinary meeting for feasibility of salvage surgery. Patients were followed up for a total of 2 years within this study.

PET/CT image acquisition

^{18}F -FDG-PET/CT studies were acquired using Phillips Gemini (London) and Siemens mCT (Sutton) PET/CT scanners. Patients were fasted for 6 h before the study. The ^{18}F -

FDG dose was determined according to EARL guidelines [3] and was administered intravenously if the blood sugar level was <10 mmol/L. Subsequently, patients rested for 60 min. Patients were positioned on a flat-top couch in the radiotherapy treatment position, using a headrest and 5-point thermoplastic shell. Unenhanced, low-dose CT was performed from the vertex to carina for purposes of attenuation correction and image fusion for anatomical localisation (approximate mAs 50/slice). FDG emission data were acquired from the vertex to carina (3 min/bed; average 2-bed acquisition).

MRI image acquisition

All MRI scans were acquired on a 1.5-T scanner (MAGNETOM Aera, Siemens Healthcare, Erlangen, Germany). Patients were set up on a flat-top MRI couch in the radiotherapy treatment position, using a headrest and 5-point thermoplastic shell. A large flex and spine coils were used. For all images, a 200 × 200-mm field of view (FOV), 2-mm isotropic voxel size and 80-mm cranio-caudal coverage was used. Anatomical T₂-weighted [echo time/repetition time (TE/TR): 82/11000 ms] and T₁-weighted (TE/TR: 13/794 ms) were acquired first to aid functional MRI planning. DW-MRI sequences [SE-EPI DWI, TE/TR: 61/13400, b values: 50, 400 and 800 s/mm², monopolar diffusion gradients, number of signal averages (NSA) = 5, bandwidth (BW) = 1000 Hz, matrix 96] were then acquired.

T₂* (R₂* = 1/T₂*) was measured using a 2D gradient echo sequence with eight echo times [flip angle (FA) = 24, TE 4.76 to 38.08 ms in increments of 4.76 ms,

TR = 1990 ms, BW = 400 Hz]. The DCE protocol included a trans-axial 3D spoiled fast gradient echo sequence with DIXON fat and water signal separation and TWIST under-sampling [TE = 2.4 and 4.8 ms, TR = 7.2 ms, BW = 450 Hz, TWIST A&B = 33%, CAIPIRHNA (R = 4)]. A series of 12 proton density-weighted images (FA = 4°) was initially acquired, followed by 100 T₁-weighted acquisitions (FA = 24°) obtained sequentially with 2-s temporal resolution. Gadolinium (Gd) contrast agent was administered intravenously at the start of the 11th dynamic scan as a bolus through a peripherally placed cannula using an automatic injector (0.2 mL/kg body mass, 2-mL/s injection rate; Dotarem, Guerbet, France) and followed by a saline flush (20 mL at 2 mL/s). A full blood count was taken prior to each MRI scan to determine blood hematocrit levels.

Image analysis

Both PET and MRI data were analyzed using RayStation (version 4.9.9, RaySearch Medical Laboratories, AB Stockholm, Sweden), a radiotherapy treatment planning system. Regions of interest (ROIs) encompassing the primary tumor (PT) or/and involved lymph nodes (LNs) were delineated on each

imaging modality by a radiation oncologist (KW). These contours were verified by respective consultants in nuclear medicine (WO) and radiology (AR). LNs included in the analysis were either proven via cytology/histology results or deemed to be unequivocally involved based on both anatomical and functional imaging characteristics following consensus among investigators.

PET images reconstructed using ordered subset expectation maximization were used for analysis. A relative threshold of 40% of the maximum standardized uptake volume (SUV_{max}) was used to generate the metabolic tumor volume ($MTV_{40\%}$). The baseline value served as the threshold for MTV on subsequent scans. PET parameters including SUV_{max} and total lesion glycolysis ($TLG_{40\%} = SUV_{mean} \times MTV_{40\%}$) [4], were recorded for all ROIs at each time point.

Anatomical contours for MRI were delineated on T_2 -weighted images with reference to T_1 -weighted images. For DW analysis, ROIs were defined on the T_2 -weighted low-b value images (b50) with reference to the co-registered anatomical contours, excluding regions of macroscopic necrosis and cystic change. All b values were used to calculate the apparent diffusion coefficient (ADC). Signal changes on multiple-gradient echo images were used to produce spatial R_2^* parametric maps. Signal intensity decay measured for increasing echo times was fitted on a voxel-by-voxel basis to a monoexponential model using a least-squares fit method. This was performed using in-house MatLab software (MathWorks, Natick, MA, USA). The DCE data were analyzed using the MRIW software package developed by The Institute of Cancer Research (ICR) [5]. The extended Kety model [6] and a population-based arterial input function [7] were used to derive a set of parameters, including the volume transfer constant between blood plasma and extracellular extravascular space (K^{trans}), the total extracellular extravascular space volume fraction (V_e) and the total blood plasma volume fraction (V_p). For SW and DCE analysis, ROIs were defined on co-registered T_1 post-Gd images.

Due to the skewed distribution of parameter values, the median was chosen as the statistical representation for each individual ROI. The fractional changes in FMI parameters from baseline [$\Delta = (x - baseline)/baseline$] were calculated for each scanning time point. The corresponding radiotherapy planning CT and dosimetry were also imported to enable dosimetric analysis.

Statistical analysis

The data were analyzed using SPSS statistical software (Version 24.0; IBM Corp, Armonk, NY, USA). The fractional changes in FMI parameters at week 1 and week 2 were compared between responders and non-responders using the Mann–Whitney U test. Categorical data were compared between the two groups using the Pearson Chi-squared test. The

significance threshold was set at $p < 0.05$. Receiver operator characteristic (ROC) analysis was used to identify and determine the optimal threshold values for parameters with predictive value.

Results

Clinical characteristics

Following exclusion of 5 patients who failed to undergo intra-treatment scans, 35 patients were available for analysis. The main reason for non-attendance was treatment-induced acute side-effects. The average times from start of CRT to scanning time points for week 1 and week 2 were 6.4 ± 1.0 days and 13.3 ± 1.0 days, respectively. Patient and tumor characteristics are summarized in Table 1. All patients completed CRT within 42 days. One patient was switched from carboplatin to cetuximab due to suboptimal renal function. The median follow-up was 14 months (range 5–33).

Treatment outcome

There were 27 responders and 8 non-responders: 5 non-responders had locoregional failure only, 2 had both

Table 1 Summary of patient and tumor characteristics

Number of patients	35
Age (y), median (range)	61 (34–69)
Sex (%)	
Male	35 (100)
Female	0 (0)
Primary location (%)	
Oropharynx	29 (83)
Hypopharynx/larynx	6 (17)
HPV status (%)	
Positive	22 (63)
Negative	13 (37)
T classification (%)	
1–2	20 (57)
3–4	15 (43)
N classification (%)	
0–1	12 (34)
2–3	23 (66)
Concomitant chemotherapy (%)	
Cisplatin	15 (43)
Carboplatin	10 (28)
Cis/carbo*	9 (26)
Cetuximab	1 (3)

*Cisplatin on day 1 switched to carboplatin on day 29

locoregional and distant failure and 1 had distant metastases without any detectable disease above the clavicles. Review of the radiotherapy dosimetry in the non-responders with locoregional persistence/recurrence revealed that all failures were in-field, i.e. within clinical target volume receiving 65 Gy. Only one non-responder was deemed suitable for salvage surgery and underwent total laryngectomy with bilateral neck dissection. That patient remains disease-free to date. Four non-responders had died at the time of analysis (5–15 months post-CRT).

Responders versus non-responders

In this cohort, treatment-induced changes in anatomical tumor volume in the first 2 weeks of CRT failed to discriminate responders from non-responders (Supplementary Table 1). Similar negative results were seen for clinical characteristics such as HPV status and T and N classification ($p > 0.05$, Supplementary Table 2).

Responders showed a greater reduction in tumor $TLG_{40\%}$ ($p = 0.007$) and SUV_{max} ($p = 0.034$) after week 1 of CRT than non-responders (Table 2). These differences between the two groups, however, disappeared by week 2. When the data were separately analyzed per PT and LNs, similar trends were observed but these failed to reach statistical significance.

The fractional changes in functional MRI parameters during CRT are summarized in Table 3. Responders showed a larger fractional increase in PT ADC values at week 2 than non-responders ($33.7 \pm 15.1\%$ versus $11.0 \pm 9.0\%$, $p < 0.001$). Whilst there was a similar trend at week 1, it was not discriminative between responders and non-responders. An example of serial changes in PT ADC is illustrated in Fig. 1. In addition, significantly larger increases in PT K^{trans} ($p = 0.012$) and V_e ($p = 0.047$) at week 2 were observed in responders (Fig. 2). Similarly, the differences in these parameters between the two groups were absent at week 1.

Conversely, the changes in R_2^* early during CRT appeared random with no apparent trend (Supplementary Fig. 1). Whilst

Table 2 Comparison of PET parameters between responders and non-responders ($n = 35$)

FMI parameters	Responders (%)	Non-responders (%)	<i>p</i> value	ROC (AUC)
Combined (PT + LNs)				
$TLG_{40\%}$ (g)				
Baseline	112.4 ± 98.2	264.7 ± 361.0%	0.192	–
Δ post-wk 1	–56.3 ± 31.0	–18.0 ± 38.8	0.007*	0.825
Δ post-wk 2	–68.7 ± 20.9	–48.8 ± 33.3	0.131	–
SUV_{max}				
Baseline	14.2 ± 5.2	16.6 ± 5.9	0.269	–
Δ post-wk 1	–27.8 ± 21.1	–8.1 ± 18.8	0.034*	0.764
Δ post-wk 2	–32.5 ± 23.0	–21.4 ± 19.8	0.158	–
Primary tumor (PT)				
$TLG_{40\%}$ (g)				
Baseline	87.8 ± 80.1	233.5 ± 291.2	0.104	–
Δ post-wk 1	–41.3 ± 23.5	–18.3 ± 37.7	0.069	–
Δ post-wk 2	–60.2 ± 17.1	–48.2 ± 34.9	0.310	–
SUV_{max}				
Baseline	14.7 ± 4.7	16.4 ± 6.1	0.498	–
Δ post-wk 1	–20.6 ± 12.7	–4.9 ± 18.5	0.050	–
Δ post-wk 2	–27.7 ± 14.7	–20.5 ± 18.0	0.224	–
Lymph nodes (LNs)				
$TLG_{40\%}$ (g)				
Baseline	50.6 ± 57.8	70.9 ± 88.4	0.532	–
Δ post-wk 1	–56.5 ± 39.5	–16.6 ± 50.9	0.085	–
Δ post-wk 2	–65.6 ± 28.2	–52.9 ± 45.6	0.790	–
SUV_{max}				
Baseline	10.9 ± 5.1	11.8 ± 5.2	0.859	–
Δ post-wk 1	–32.1 ± 24.1	–18.8 ± 16.6	0.391	–
Δ post-wk 2	–34.8 ± 28.1	–34.9 ± 12.2	0.533	–

*Statistically significant difference

Table 3 Comparison of MRI parameters between responders and non-responders (n = 35)

FMI parameters	Responders (%)	Non-responders (%)	p value	ROC (AUC)
Primary (27 ROIs)				
ADC ($\times 10^{-3}$ mm ² /s)				
Baseline	1.02 \pm 0.19	1.22 \pm 0.14	0.009*	0.829
Δ post-wk 1	18.9 \pm 25.5	5.1 \pm 33.7	0.274	–
Δ post-wk 2	33.7 \pm 15.1	11.0 \pm 9.0	0.000*	0.937
R ₂ * (s ⁻¹)				
Baseline	34.3 \pm 10.5	31.4 \pm 10.0	0.685	–
Δ post-wk 1	0.7 \pm 23.6	-5.3 \pm 25.6	0.555	–
Δ post-wk 2	-5.3 \pm 25.6	4.0 \pm 25.4	0.791	–
K ^{trans} (min ⁻¹)				
Baseline	0.202 \pm 0.040	0.194 \pm 0.049	0.735	–
Δ post-wk 1	47.3 \pm 41.6	28.2 \pm 27.3	0.331	–
Δ post-wk 2	115.4 \pm 117.2	13.9 \pm 51.2	0.012*	0.813
V _e				
Baseline	0.256 \pm 0.055	0.318 \pm 0.055	0.003*	0.864
Δ post-wk 1	6.9 \pm 5.9	8.1 \pm 22.9	0.836	–
Δ post-wk 2	12.9 \pm 9.8	0.1 \pm 16.6	0.047*	0.774
V _p ($\times 10^{-3}$)				
Baseline	8.5 \pm 7.4	2.7 \pm 5.6	0.072	–
Δ post-wk 1	-0.52 \pm 0.73	-0.03 \pm 0.86	0.219	–
Δ post-wk 2	-0.53 \pm 0.75	-0.16 \pm 2.06	0.288	–
Lymph nodes (36 ROIs)				
ADC ($\times 10^{-3}$ mm ² /s)				
Baseline	1.059 \pm 0.211	1.086 \pm 0.091	0.456	–
Δ post-wk 1	13.6 \pm 12.2	18.0 \pm 7.4	0.239	–
Δ post-wk 2	33.4 \pm 19.0	30.1 \pm 4.4	0.900	–
R ₂ * (s ⁻¹)				
Baseline	20.7 \pm 4.7	21.1 \pm 2.3	0.611	–
Δ post-wk 1	3.8 \pm 18.4	4.5 \pm 10.8	0.677	–
Δ post-wk 2	4.4 \pm 23.0	7.4 \pm 8.3	0.445	–
K ^{trans} (min ⁻¹)				
Baseline	0.167 \pm 0.044	0.204 \pm 0.81	0.184	–
Δ post-wk 1	45.5 \pm 42.5	64.6 \pm 96.4	1.000	–
Δ post-wk 2	34.5 \pm 59.7	-5.0 \pm 31.3	0.102	–
V _e				
Baseline	0.241 \pm 0.079	0.339 \pm 0.120	0.020*	0.783
Δ post-wk 1	6.8 \pm 7.1	13.8 \pm 14.7	0.244	–
Δ post-wk 2	11.9 \pm 10.3	8.5 \pm 4.3	0.694	–
V _p ($\times 10^{-3}$)				
Baseline	4.5 \pm 5.2	1.1 \pm 2.6	0.229	–
Δ post-wk 1	-0.18 \pm 0.50	-0.13 \pm 0.28	0.944	–
Δ post-wk 2	-0.12 \pm 0.67	-0.10 \pm 0.30	0.813	–

*statistically significant difference

there was a trend for a larger decrease in PT V_p in responders, this did not reach statistical significance. No significant intra-treatment changes were detected in LNs for all functional MRI parameters; however, the trends were consistent for those for PTs.

ROC analysis identified changes in PT ADC at week 2 as the most powerful predictor of response to CRT with AUC of 0.937. An increase in PT ADC >17% at week 2 has a sensitivity, specificity and accuracy of 100%, 86% and 96%, respectively, in predicting response following CRT. For earlier

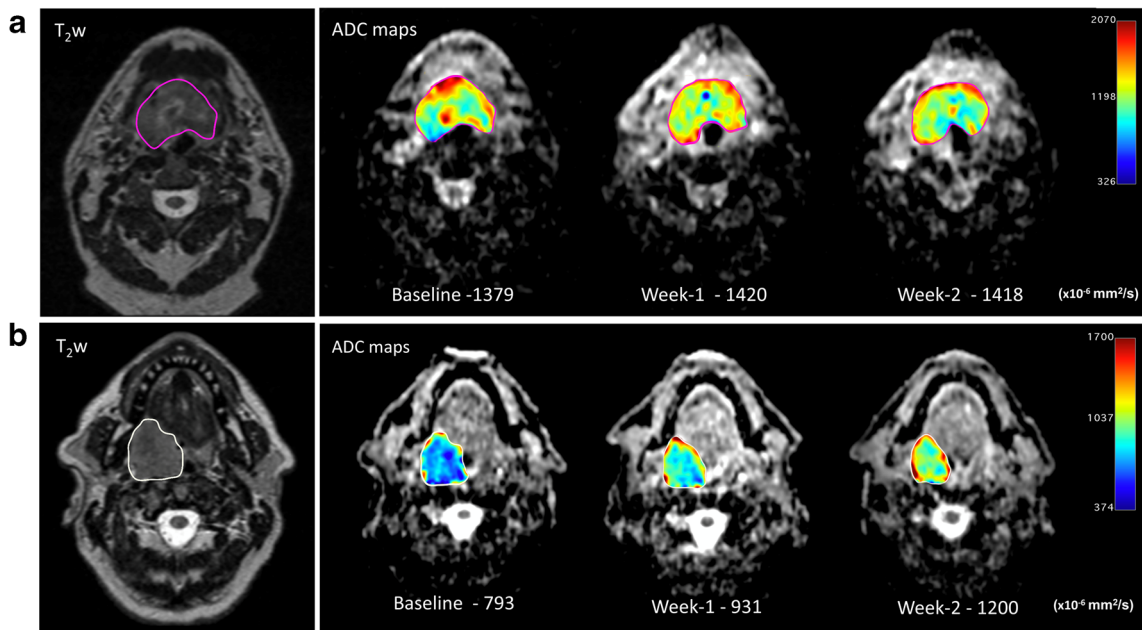


Fig. 1 Serial ADC maps (tumor ROI displayed in jet color scale) in the first 2 weeks of CRT for **A** (non-responder) and **B** (responder). Patient B showed a large treatment-induced increase in PT ADC (+51.3% post-week 2) in contrast to patient A (+2.8% post-week 2)

assessment at week 1, total $TLG_{40\%}$ was the parameter of choice with a reduction of >12%, giving a sensitivity and specificity of 93% and 83%, respectively, in predicting

treatment response. Attempts to combine the strongest predictor, ADC, with other FMI parameters did not further improve its performance.

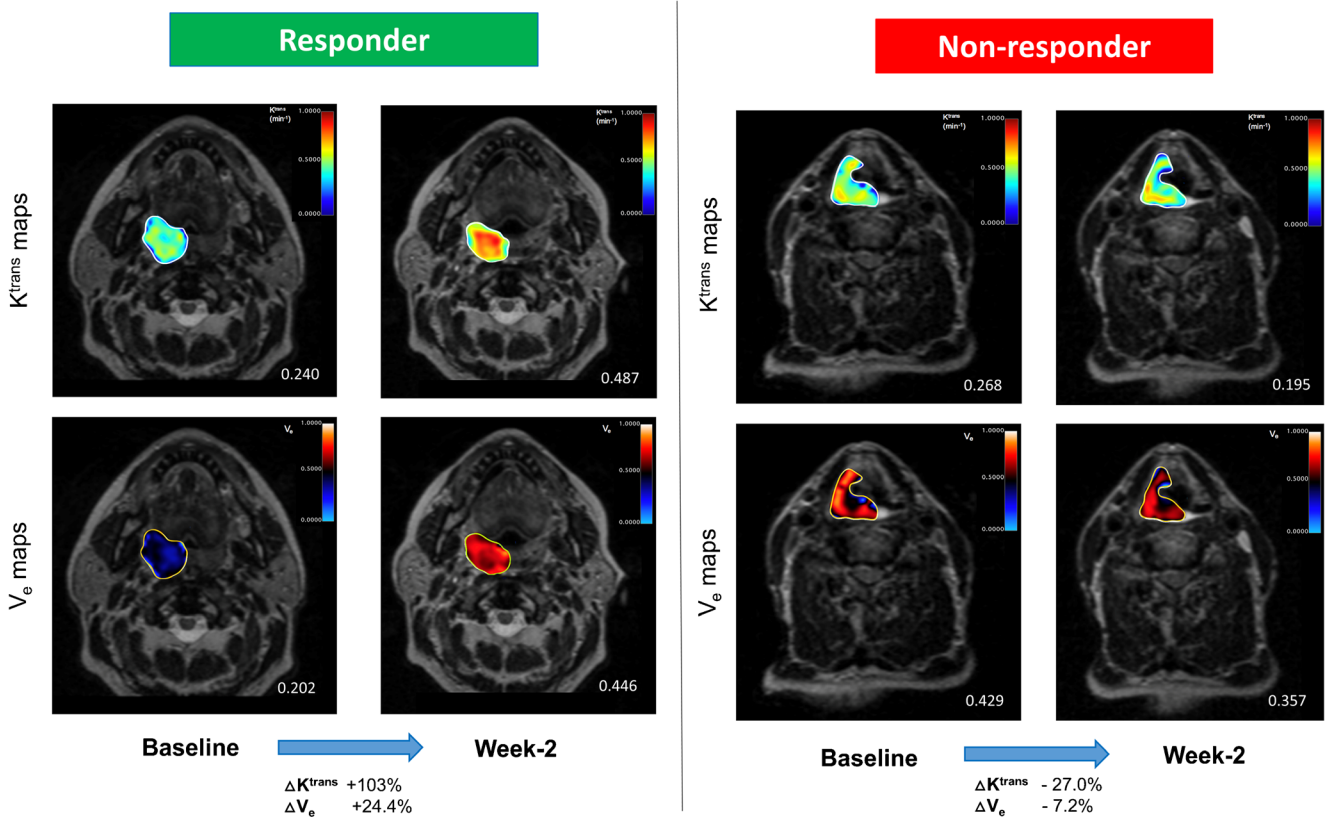


Fig. 2 Overlay K^{trans} and V_e maps demonstrating the differences in longitudinal changes between responder and non-responder after week 2 of CRT. The responder showed a significantly larger increase in median K^{trans} and V_e , in comparison to the non-responder

Discussion

We evaluated early intra-treatment assessment using multimodality FMI parameters to predict response to CRT in patients with locally advanced HNSCC. The reason for investigating the chosen study time points and not later, i.e. >2 weeks, is to allow early identification of patients who are likely or unlikely to respond so that the window of opportunity to affect therapeutic outcome is not missed. Responders could be considered for treatment de-escalation, e.g. radiotherapy dose reduction or target volume adaptation, to reduce treatment-related morbidity [8, 9]. In contrast, non-responders should be considered for treatment intensification, e.g. radiotherapy dose escalation [10], hypoxia modification [11], novel radiosensitisers [12, 13] and/or ‘bail out’ surgery.

As shown in previous studies [14, 15], treatment-induced changes in FMI parameters precede anatomical changes, allowing earlier risk stratification of patients. Our data demonstrated differing optimal times for early response assessment during CRT when FDG-PET and MRI parameters were used. Changes in tumor $TLG_{40\%}$ and SUV_{max} at week 1 were predictive of treatment outcome, but these signals, in fact, disappeared later by week 2. This was explained by the low tumor FDG uptake and lesser difference between the two groups by week 2. Another possible confounding factor is the influence of radiotherapy-induced peritumoral inflammation on FDG uptake with cumulative fractions, which may affect ROI segmentation (Fig. 3), but this phenomenon is typically observed during the latter part of radiotherapy [2, 16]. This raises uncertainties about the reliability of FDG-PET parameters in reflecting tumor response beyond the first week of CRT. It is also evident that combined, rather than isolated, analysis of PT and LN FDG-PET parameters provides a better overall representation of the tumor response. To the best of our knowledge, this is the first published data investigating the predictive value of early intra-treatment changes in FDG-PET parameters in such a setting.

In contrast to FDG-PET parameters, it was not until week 2 that treatment-induced changes in MRI parameters successfully

discriminated responders from non-responders. Our data showed that a larger fractional increase in PT DW-derived ADC at week 2 ($\Delta > 17\%$) was highly predictive of favorable response to CRT. Overall, our results are consistent with previous DW MRI studies which cumulatively reported that an increase of tumor ADC (>14–24%) between week 1 and 4 of radiotherapy could predict treatment outcome [17–20]. Kim et al. reported intra-treatment assessment at week 1 to be predictive of response, but their scans were performed on average 12 days after the start of CRT [19], which would have been defined as week 2 in our study. Thus, it is reasonable to deduce that whilst highly desirable, earlier assessment with DW MRI (e.g. <7 days from start of CRT) is premature and of limited utility in HNSCC. Moreover, our study improves on previous studies due to its homogeneity: previous studies used MRI of different strengths (1.5 and 3 T) within the same study, had less standardized scanning time points (standard deviation of >3 days) or/and included patients with early disease (stage I-II) undergoing radiotherapy only.

We also found responders to have a larger fractional increase in PT DCE-derived K^{trans} and V_e . Similarly, these were only evident by week 2. These observations are likely to reflect early cell degradation in responding tumors, resulting in expansion of interstitial space and increased vascular permeability. Unlike DW MRI, there is limited data on the role of intra-treatment DCE MRI to assess and predict response to CRT. This may be related to the technical difficulties, e.g. tumor motion due to swallowing and workload required to process DCE data. We are aware of only two pilot studies which assessed changes in DCE parameters during radical radiotherapy in patients with HNSCC. Cao et al. reported an increase in PT blood volume (BV) 2 weeks into CRT to be associated with local control [21]. Baer et al. subsequently investigated a novel method of using parametric response maps of DCE MRI to predict survival following CRT in 10 patients: they found patients with a large percentage of PT gross volume that decreased in K^{trans} after 2 weeks were more likely to have significantly reduced survival [22]. Our larger study supported their findings that intra-treatment changes in K^{trans} is a potential biomarker in predicting treatment response.

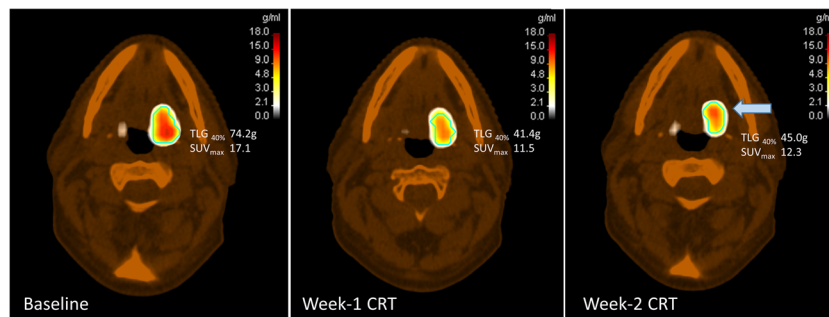


Fig. 3 An example of a responder having a paradoxical increase in primary tumor SUV at week 2 (highlighted by the blue arrow, cyan contour = $MTV_{40\%}$) despite a marked initial decrease at week 1. This

phenomenon was observed in a few other responders, which may be confounded by radiotherapy-induced peritumoral inflammation with cumulative fractions

In this study, we also investigated the role of SW-derived R_2^* as a predictive biomarker in HNSCC. SW MRI is an alternative, hypoxia-dependent, non-invasive imaging technique that exploits the paramagnetic properties of deoxyhaemoglobin in erythrocytes to create contrast. Our interest in SW MRI stems from pre-clinical data [23] and a previous clinical study in cervical cancer demonstrating the ability of baseline tumor R_2^* to predict response to CRT: responders had a lower average baseline R_2^* than non-responders [24]. This result was not replicated in our study and we did not find any apparent trends for alterations in R_2^* during the first 2 weeks of CRT. The only other R_2^* study in HNSCC was recently published by Min et al. and they also failed to demonstrate any clear pattern in its weekly changes throughout radiotherapy [25]. They did not correlate R_2^* with treatment outcome, but as with our observation, it was evident that R_2^* does not appear to have a predictive role in HNSCC as a standalone parameter. A possible explanation is that R_2^* values are strongly dependent on tumor BV [26, 27], which is highly heterogeneous in HNSCC. An accurate and robust measurement of tumor BV is challenging [28, 29]. Therefore, additional work is required to ascertain how best to interpret R_2^* measurements with BV before it can be utilized as a hypoxia imaging biomarker in HNSCC.

Attempts to combine multiple identified FMI parameters failed to yield superior predictive power over a single parameter (ΔADC at week 2) in this cohort. This may partly be due to the relatively small number of non-responders in our study (8/35, 23%). The risk of treatment failure is not truly binarised by a single parameter threshold, and in 'real-life' clinical practice, intra-treatment changes in other predictive parameters (TLG_{40%}, K^{trans} and V_e) may prove useful in further determining the risk in equivocal cases. Our study has provided the basic framework for early intra-treatment assessment with FMI in locally advanced HNSCC, but requires further refinement and validation with more patients. This work continues and we are expanding our PET and functional MRI database beyond the current study cohort.

There are limitations of this study. Eight patients with T1–2 tonsillar cancer did not have measurable PT following diagnostic tonsillectomy and it is unclear whether this would have an impact on the result. In addition, the cranio-caudal coverage of our MRI protocol meant that in five patients, involved LNs outside the FOV were excluded. However, the largest LN for each patient was included, which is likely to have been representative of the dominant tumor biology. Another difficulty was the requirement to exclude obviously necrotic or cystic regions of the tumor, which was performed manually.

Conclusion

Our study highlighted the importance of intra-treatment scanning time points when integrated into clinical practice due to its impact on prediction outcome. This study provides the

framework of utilizing multimodality FMI early during CRT and could be used to inform the design of future risk-stratified adaptive interventional studies in HNSCC.

Acknowledgments This work was undertaken in The Royal Marsden NHS Foundation Trust who received a proportion of its funding from the NHS Executive; the views expressed in this publication are those of the authors and not necessarily those of the NHS Executive. We acknowledge the support of the National Institute for Health Research, Royal Marsden and Institute of Cancer Research Clinical Research Facility in Imaging and the Biomedical Research Centre. SAB, CMN, KJH and KLN acknowledge research support from Oracle Cancer Trust. MOL is an NIHR Emeritus Senior Investigator. We also thank the radiographers, nuclear medicine technicians and research nurses (Tara Hurley, Loma Grove, Motoko Ryugenji and Ana Santos) for their support.

Funding This study was funded by Cancer Research UK Head and Neck programme grants C7224/A13407 and C7224/A23275. It was also supported by Cancer Research UK to CRUK Imaging Centre, grant numbers C1060/A10334 and C1060/A16464.

Compliance with ethical standards

Conflict of interest None declared by all authors.

Ethical approval The Institutional Review Board (CCR3926) and Research Ethical Committee (13/LO/0067) approved this study (NCRI H&N CSG ID 13860). All procedures performed in this study were in accordance with the ethical standards of the institutional and national research committee and with the 1964 Helsinki Declaration and its later amendments or comparable ethical standards.

Informed consent Written consents were obtained from all individual participants in this study.

Open Access This article is distributed under the terms of the Creative Commons Attribution 4.0 International License (<http://creativecommons.org/licenses/by/4.0/>), which permits unrestricted use, distribution, and reproduction in any medium, provided you give appropriate credit to the original author(s) and the source, provide a link to the Creative Commons license, and indicate if changes were made.

References

1. Han M, Kim SY, Lee SJ, Choi JW. The correlations between MRI perfusion, diffusion parameters, and 18F-FDG PET metabolic parameters in primary head-and-neck cancer: a cross-sectional analysis in single institute. *Medicine (Baltimore)*. 2015;94:e2141.
2. Subesinghe M, Scarsbrook AF, Sourbron S, Wilson DJ, McDermott G, Speight R, et al. Alterations in anatomic and functional imaging parameters with repeated FDG PET-CT and MRI during radiotherapy for head and neck cancer: a pilot study. *BMC Cancer*. BioMed Central Ltd. 2015;15:137.
3. Boellaard R, Delgado-Bolton R, Oyen WJG, Giammarile F, Tatsch K, Eschner W, et al. FDG PET/CT: EANM procedure guidelines for tumor imaging: version 2.0. 2nd ed. *Eur J Nucl Med Mol Imaging*. 2015;328–54.
4. Larson SM, Erdi Y, Akhurst T, Mazumdar M, Macapinlac HA, Finn RD, et al. Tumor treatment response based on visual and quantitative changes in global tumor Glycolysis using PET-FDG imaging.

- The visual response score and the change in Total lesion Glycolysis. *Clin Positron Imaging*. 1999;2:159–71.
5. d'Arcy JA, Collins DJ, Padhani AR, Walker-Samuel S, Suckling J, Leach MO. Informatics in radiology (infoRAD): magnetic resonance imaging workbench: analysis and visualization of dynamic contrast-enhanced MR imaging data. *Radiographics*. 2005;26:621–32.
 6. Tofts PS, Brix G, Buckley DL, Evelhoch JL, Henderson E, Knopp MV, et al. Estimating kinetic parameters from dynamic contrast-enhanced T1-weighted MRI of a diffusable tracer: standardized quantities and symbols. *J Magn Reson Imaging*. 1999;10:223–32.
 7. Orton MR, d'Arcy JA, Walker-Samuel S, Hawkes DJ, Atkinson D, Collins DJ, et al. Computationally efficient vascular input function models for quantitative kinetic modelling using DCE-MRI. *Phys Med Biol*. 2008;53:1225–39.
 8. Chen AM, Felix C, Wang PC, Hsu S, Basehart V, Garst J, et al. Reduced-dose radiotherapy for human papillomavirus-associated squamous-cell carcinoma of the oropharynx: a single-arm, phase 2 study. *Lancet Oncol*. 2017;18(6):803–11.
 9. Kataria T, Gupta D, Goyal S, Bisht SS, Basu T, Abhishek A, et al. Clinical outcomes of adaptive radiotherapy in head and neck cancers. *BJR*. 2016;89:20160085–6.
 10. Pigorsch SU, Wilkens JJ, Kampfer S, Kehl V, Hapfelmeier A, Schläger C, et al. Do selective radiation dose escalation and tumor hypoxia status impact the loco-regional tumor control after radiochemotherapy of head & neck tumors? The ESCALOX protocol. *Radiat Oncol*. 2017;12(1):45.
 11. Bentzen J, Toustrup K, Eriksen JG, Primdahl H, Andersen LJ, Overgaard J. Locally advanced head and neck cancer treated with accelerated radiotherapy, the hypoxic modifier nimorazole and weekly cisplatin. Results from the DAHANCA 18 phase II study. *Acta Oncol*. 2015;54:1001–7.
 12. Nickson CM, Moori P, Carter RJ, Rubbi CP. Misregulation of DNA damage repair pathways in HPV-positive head and neck squamous cell carcinoma contributes to cellular radiosensitivity. *Oncotarget*. 2017.
 13. Nagasaka M, Zaki M, Kim H, Raza SN, Yoo G, Lin H-S, et al. PD1/PD-L1 inhibition as a potential radiosensitizer in head and neck squamous cell carcinoma: a case report. *J Immunother Cancer*. 2016;4:83.
 14. Wong KH, Panek R, Welsh L, McQuaid D, Dunlop A, Riddell A, et al. The predictive value of early assessment after 1 cycle of induction chemotherapy with 18F-FDG PET/CT and diffusion-weighted MRI for response to radical Chemoradiotherapy in head and neck Squamous cell carcinoma. *J Nucl Med*. 2016;57:1843–50.
 15. Powell C, Schmidt M, Borri M, Koh D-M, Partridge M, Riddell A, et al. Changes in functional imaging parameters following induction chemotherapy have important implications for individualised patient-based treatment regimens for advanced head and neck cancer. *Radiother Oncol*. 2013;106:112–7.
 16. Troost EGC, Bussink J, Hoffmann AL, Boerman OC, Oyen WJG, Kaanders JHAM. 18F-FLT PET/CT for early response monitoring and dose escalation in oropharyngeal tumors. *J Nucl Med*. 2010;51:866–74.
 17. King AD, Mo FKF, Yu K-H, Yeung DKW, Zhou H, Bhatia KS, et al. Squamous cell carcinoma of the head and neck: diffusion-weighted MR imaging for prediction and monitoring of treatment response. *Eur Radiol*. 2010;20:2213–20.
 18. Matoba M, Tuji H, Shimode Y, Toyoda I, Kuginuki Y, Miwa K, et al. Fractional change in apparent diffusion coefficient as an imaging biomarker for predicting treatment response in head and neck cancer treated with chemoradiotherapy. *AJNR Am J Neuroradiol*. 2014;35:379–85.
 19. Kim S, Loevner L, Quon H, Sherman E, Weinstein G, Kilger A, et al. Diffusion-weighted magnetic resonance imaging for predicting and detecting early response to chemoradiation therapy of squamous cell carcinomas of the head and neck. *Clin Cancer Res*. 2009;15:986–94.
 20. Vandecaveye V, Dirix P, De Keyser F, Op de Beeck K, Vander Poorten V, Hauben E, et al. Diffusion-weighted magnetic resonance imaging early after chemoradiotherapy to monitor treatment response in head-and-neck squamous cell carcinoma. *Int J Radiat Oncol Biol Phys*. 2012;82:1098–107.
 21. Cao Y, Popovtzer A, Li D, Chepeha DB, Moyer JS, Prince ME, et al. Early prediction of outcome in advanced head-and-neck cancer based on tumor blood volume alterations during therapy: a prospective study. *Int J Radiat Oncol Biol Phys*. 2008;72:1287–90.
 22. Baer AH, Hoff BA, Srinivasan A, Galban CJ, Mukherji SK. Feasibility analysis of the parametric response map as an early predictor of treatment efficacy in head and neck cancer. *AJNR Am J Neuroradiol*. 2015;36:757–62.
 23. Baudelet C, Gallez B. How does blood oxygen level-dependent (BOLD) contrast correlate with oxygen partial pressure (pO₂) inside tumors? *Magn Reson Med*. 2002;48:980–6.
 24. Li XS, Fan HX, Fang H, Song YL, Zhou CW. Value of R2* obtained from T2*-weighted imaging in predicting the prognosis of advanced cervical squamous carcinoma treated with concurrent chemoradiotherapy. *J Magn Reson Imaging*. 2015;42:681–8.
 25. Min M, Lee MT, Lin P, Holloway L, Wijesekera D, Gooneratne D, et al. Assessment of serial multi-parametric functional MRI (diffusion-weighted imaging and R2*) with 18F-FDG-PET in patients with head and neck cancer treated with radiation therapy. *BJR*. 2016;89:20150530–9.
 26. Panek R, Welsh L, Dunlop A, Wong KH, Riddell AM, Koh D-M, et al. Repeatability and sensitivity of T2* measurements in patients with head and neck squamous cell carcinoma at 3T. *J Magn Reson Imaging*. 2016;44:72–80.
 27. Rodrigues LM, Howe FA, Griffiths JR, Robinson SP. Tumor R2* is a prognostic indicator of acute radiotherapeutic response in rodent tumors. *J Magn Reson Imaging*. 2004;19:482–8.
 28. Dennie J, Mandeville JB, Boxerman JL, Packard SD, Rosen BR, Weisskoff RM. NMR imaging of changes in vascular morphology due to tumor angiogenesis. *Magn Reson Med*. 1998;40:793–9.
 29. Gambarota G, van Laarhoven HWM, Philippens M, Lok J, van der Kogel A, Punt CJA, et al. Assessment of absolute blood volume in carcinoma by USPIO contrast-enhanced MRI. *Magn Reson Imaging*. 2006;24:279–86.